IOP Conf. Series: Journal of Physics: Conf. Series **1489** (2020) 012011 doi:10.1088/1742-6596/1489/1/012011

Modelling Steady Convection-Dominated Phenomena by Node-Adaptive Radial Point Interpolation Meshfree Method (RPIM) with Various RBFs

K Chanthawara[1,*] **and S Kaennakham**[2,3]

[1] Program of Mathematics, Faculty of Science, Ubon Ratchathani Rajabhat University, Mueang Ubon Ratchathani, Ubon Ratchathani 34000, Thailand.
[2] School of Mathematics, Institute of Science, Suranaree University of Technology, Nakhon Ratchasima 30000, Thailand.
[3] Centre of Excellence in Mathematics, Bangkok 10400, Thailand.
[*] Corresponding Author: Krittidej Chanthawara. Email: krittidej.c@ubru.ac.th

Abstract. For numerically solving PDEs, node or grid adaptation schemes have been invented, applied, and improved mainly to improve solution accuracy while reducing the burden caused by CPU-limitation and/or users' interference. This becomes crucial particularly for problems involving strong changes in physical phenomena. This work proposes a means of node-adaptation used in conjunction with a numerical meshfree method called 'radial point interpolation (RPIM)', carried out using the concept of interpolation via. radial basis functions and hence no grid or mesh required. The proposed method is developed to tackle one of the most challenging problems with convective force being overwhelming in the system. This phenomena is known not to be easily numerically simulated. The proposed node-adaptive scheme is carried out where locally-estimated Péclet number (Pe) being used to indicate the areas of interest, places where nodes are expected to be added or removed. The whole adaptation algorithm is dynamic requiring on user's interference. When compared to solutions obtained from fixed-node cases and other benchmark work, the results obtained in this work strongly suggest benefits in terms of both solution accuracy improvement and CPU-storage reduction.

1. Introduction

Appearing in many branches of sciences and engineering such as biological, physical chemical, physical in fluid mechanics, astrophysics, meteorology, and multiphase flow in oil reservoirs, polymer flow [1], convection-diffusion type of PDE is known to play important roles. The combination of two phenomena; convection and diffusion is widely regarded as a great challenge when finding solutions both analytically and numerically. The case becomes even more challenging when the convective force becomes dominant and one often meets with situations where thin boundary and interior layers are presented and singular perturbation problems arises known as 'convection-dominated' phenomena. A number of investigations have been carried out over the decades to provide reliable solutions and/or treatments for modelling the phenomena [2]. Some recent works include the use of Meshless local Petrov–Galerkin (MLPG) method done in [3], several numerical techniques; the enlargement of the local support domain, the upwind support domain, the adaptive upwind support domain, the biased support domain, the nodal refinement, and the adaptive analysis, as presented in [4], a stencil of the finite–difference method [5], the traditional global collocation Kansa method [6], and the dual reciprocity boundary element method [7].

On the development of numerical methods, a new class of numerical methods known as 'meshless / meshfree' has recently been receiving great amount of interest from scientists and engineers. Some different versions of this kind are the element-free Galerkin method [8, 9], the local Petrov-Galerkin [10,11], and meshless manifold method [12], (please also see references therein). Along this track, Kansa [13] was the first who performed an application of a collocation method based on Multiquadric Radial Basis Function (MQ-RBF) to a set of PDEs in 1990. There have been a great amount of attempts in developing, applying, and modifying the method to different kinds of problems ever since. This includes groundwater contaminant transport [14], plate and shell analysis [15,16,17], microelectromechanical system analysis [18] and many more.

The traditional version of Kansa, nevertheless, is known to severely suffer from having a fully unsymmetric and populated collocation matrix, increasing the risk of being ill-conditioned. The problem becomes even more severe when the number of nodes are increasing or with larger domain. One of the improved versions is the attempt to combine the radial basis function and some polynomial basis functions firstly proposed in 2002 by Wang and Liu [19], known as 'The Radial Point Interpolation Method (RPIM)'. With this method, the approximation of the solution is obtained by letting the interpolation function pass through the function values at each scattered node within the domain. Liu [20] in 2011, concluded that by using the combination of radial and polynomial basis functions, the singularity problem can be improved. Together to this, the effect of shape parameters on the method for elastoplastic problems in two-dimension models using MQ-RBF was documented by Bozkurt et al [21] in 2013. For some more recently and nicely documented, the interested reader is referred to [22] and [23].

For all collocation-based meshless methods mentioned so far, including RPIM, it is the Radial Basis Function that plays a crucial role in determining the quality of the final results. Radial Basis Functions (RBF), φ , are multivariate functions whose values are dependent only on the distance from the origin. This means that on the distance from a point of a given set $\{\mathbf{x}_j\}$, and $\varphi(\mathbf{x}-\mathbf{x}_j)=\varphi(r_j)\in\mathbb{R}$. Here, $r_j=\|\mathbf{x}-\mathbf{x}_j\|_2$ is the Euclidean distance and any function φ satisfying $\varphi(\mathbf{x})=\varphi(\|\mathbf{x}\|_2)$ is called 'a radial function'. RBFs have been receiving a great amount of interest from researchers from many branches of applications [24]. Some of the most popular choices are focussed on in this work and they are listed as follows [25];

- Multiquadric (MQ) : $\varphi(r)=\sqrt{1+(\varepsilon r)^2}$
- Gaussian (GA) : $\varphi(r)=\exp\left(-(\varepsilon r)^2\right)$
- Inverse Quadratic (IQ) : $\varphi(r)=1/\left[1+(\varepsilon r)^2\right]$
- Inverse Multiquadric (IMQ) : $\varphi(r)=1/\sqrt{1+(\varepsilon r)^2}$
- Cubic Matérn (CMT) : $\varphi(r)=\left(15+15\varepsilon r+6(\varepsilon r)^2+(\varepsilon r)^3\right)$

Where ε is the so-called 'shape parameter' and to be determined by the user. Figure 1 illustrates their surface profiles at the same $\varepsilon=10.00$.

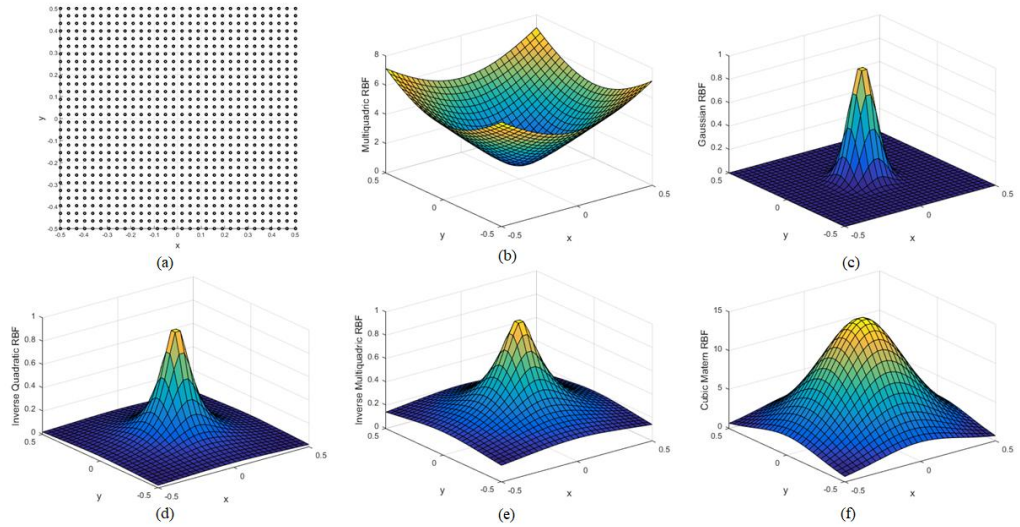

Figure 1. Radial Basis Function Profiles at $\varepsilon = 10.00$; (a) computational nodes, (b) Multiquadric (MQ), (c) Gaussian (GA), (d) Inverse Quadratic (IQ), (e) Inverse Multiquadric (IMQ), and (f) Cubic Matérn (CMT).

Last but not least, one of the objectives of this work is also to optimize the numerical process in terms of CPU-storage and time, while obtaining the optimal result quality by proposing a means of node-adaptation. The research in the area of node-adaptation or grid-adaptive schemes has been widely studied and nevertheless, most attempts have been associated with the traditional numerical methods, i.e. finite element method, finite volume method, and finite difference method, see [26]. On the other hand, only a small number of investigations done under the scope of meshfree/meshless. Some recent works include the use of wavelet based adaptive [27], the distributed adaptive node-specific signal estimation (DANSE) algorithm [28], the hybrid global RBF-meshless with minimal fine tuning [29], the use of two constraints in equidistribution algorithm [30], and the centroid-adaptive global collocation [31].

The organization of this work is as follows. The mathematical structure of the Radial Point Interpolation Method (RPIM) and the proposed-node adaptation scheme are detailed in Section 2. Its numerical implementation to the steady convection-diffusion problem is provided in Section 3. Section 4 presents the overall performance of the method via several benchmark test cases. Findings obtained are also discussed in the same section before Section 5 summarizes the main conclusions.

2. Mathematical Background

2.1. Radial Point Interpolation Meshfree (RPIM) Method

The collocation scheme starts with considering the following elliptical partial differential equation, defined on a bounded and connected domain Ω;

$$\Phi\left[u(\mathbf{x})\right] = f(x) \qquad \text{for } \mathbf{x} \in \Omega \subset \mathbb{R}^n \tag{2.1}$$

$$B_1 u(\mathbf{x}) = g(x) \qquad \text{for } \mathbf{x} \in \Gamma_1 \tag{2.2}$$

$$B_2 u(\mathbf{x}) = h(x) \qquad \text{for } \mathbf{x} \in \Gamma_2 \tag{2.3}$$

Where $\partial\Omega$ is the domain boundary containing two non-overlap sections; Γ_1 and Γ_2, with $\Gamma_1 \cap \Gamma_2 = \phi$. These differential operators; Φ, and B_1, B_2 are applied on the domain, and the two boundary sections respectively. Let $\mathbf{X}^c = \left\{\mathbf{x}_j\right\}_{j=1}^{N}$ be a set of randomly selected points, known as

'collocation' or 'centres', on the domain where $\left\{\mathbf{x}_j\right\}_{j=1}^{N_i}$ are those contained within, and $\left\{\mathbf{x}_j\right\}_{j=N_i+1}^{N_i+N_1}$ and $\left\{\mathbf{x}_j\right\}_{j=N_i+N_1+1}^{N}$ are those on the boundary Γ_1 and Γ_2 respectively.

The radial point interpolation scheme writes the approximate solution $\tilde{u}(\mathbf{x})$, as the linear combination of the basis function $\left\{\varphi(:-)\right\}_j^N$ and monomials $p_j(\mathbf{x})$, shown in the following form;

$$\begin{aligned} u(\mathbf{x}) \simeq \tilde{u}(\mathbf{x}) &= \sum_{i=1}^{N} R\left(\left\|\mathbf{x}-\mathbf{x}_i\right\|_2\right) a_i + \sum_{j=1}^{M} p_j(\mathbf{x}) b_j \\ &= \mathbf{R}^{\mathrm{T}}(\mathbf{x})\mathbf{a} + \mathbf{P}^{\mathrm{T}}(\mathbf{x})\mathbf{b} \end{aligned} \tag{2.4}$$

This is defined for N , the total number of centres, and M representing the number of polynomial basis (usually, $M < N$). The polynomial function can be chosen from Pascal's triangle which, for 2D problems, is of the following form;

$$\mathbf{P}^{\mathbf{T}}(\mathbf{x}) = \begin{bmatrix} 1 & x & y & x^2 & xy & y^2 & \ldots \end{bmatrix} \tag{2.5}$$

With this additional term, the interpolation is enforced to pass thought all those N nodes in the domain. To ensure the unique solution of the system, additional M equations are added as the constraint conditions, displayed as follows;

$$\sum_{i=1}^{N} p_j(\mathbf{x}_i) a_i = \mathbf{P}_M^{\mathrm{T}}\mathbf{a} = 0 \tag{2.6}$$

For $j = 1, 2, \ldots, M$. This leads to the following form.

$$\tilde{\mathbf{U}}(\mathbf{x}) = \begin{bmatrix} \mathbf{U}(\mathbf{x}) \\ \mathbf{0} \end{bmatrix} = \begin{bmatrix} \mathbf{R}_0 & \mathbf{P}_M \\ \mathbf{P}_M^T & \mathbf{0} \end{bmatrix} \begin{bmatrix} \mathbf{a} \\ \mathbf{b} \end{bmatrix} = \mathbf{H}\boldsymbol{\alpha}_0 \tag{2.7}$$

Leading to

$$\boldsymbol{\alpha}_0 = \mathbf{H}^{-1}\tilde{\mathbf{U}}(\mathbf{x}) \tag{2.8}$$

Where

$$\mathbf{H} = \begin{bmatrix} \mathbf{R}_0 & \mathbf{P}_M \\ \mathbf{P}_M^T & \mathbf{0} \end{bmatrix},$$

$$\boldsymbol{\alpha}_0 = \begin{bmatrix} \mathbf{a} \\ \mathbf{b} \end{bmatrix} = \begin{bmatrix} a_1 & a_2 & \ldots & a_n & b_1 & b_2 & \ldots & b_M \end{bmatrix}^T$$

$$\mathbf{R}_0 = \begin{bmatrix} R_1(x_1, y_1) & R_2(x_1, y_1) & \ldots & R_N(x_1, y_1) \\ R_1(x_2, y_2) & R_2(x_2, y_2) & \ldots & R_N(x_2, y_2) \\ \vdots & \vdots & \ddots & \vdots \\ R_1(x_N, y_N) & R_2(x_N, y_N) & \ldots & R_N(x_N, y_N) \end{bmatrix}_{N \times N}$$

$$\mathbf{P}_M^T = \begin{bmatrix} 1 & 1 & \ldots & 1 \\ x_1 & x_2 & \ldots & x_N \\ y_1 & y_2 & \ldots & y_N \\ \vdots & \vdots & \ddots & \vdots \\ p_M(\mathrm{x}_1) & p_M(\mathrm{x}_2) & \ldots & p_M(\mathrm{x}_N) \end{bmatrix}_{M \times N}$$

Substituting these back into the collocation equation, yielding;

$$u(\mathbf{x}) = \left[\mathbf{R}^{\mathrm{T}}(\mathbf{x}) \quad \mathbf{P}^{\mathrm{T}}(\mathbf{x}) \right] \mathbf{H}^{-1} \tilde{\mathbf{U}}(\mathbf{x}) \tag{2.9}$$

By setting the shape functions matrix, $\widehat{\mathbf{\Theta}}^{\mathrm{T}}(\mathbf{x})$, as;

$$\widehat{\mathbf{\Theta}}^{\mathrm{T}}(\mathbf{x}) = \left[\mathbf{R}^{\mathrm{T}}(\mathbf{x}) \quad \mathbf{P}^{\mathrm{T}}(\mathbf{x}) \right] \mathbf{H}^{-1} \tag{2.10}$$

Then the previous equation can be re-written as;

$$u(\mathbf{x}) = \widehat{\mathbf{\Theta}}^{\mathrm{T}}(\mathbf{x}) \tilde{\mathbf{U}}(\mathbf{x}) \tag{2.11}$$

2.2. The Node Adaptation Scheme

Generally, the methodology of mesh refinement/enrichment can be classified into four main groups as follows;

- **h-refinement:** nodes are added or removed from the computing domain based on some user's pre-defined refinement criteria (See [26] and references therein).
- **r-refinement:** the number of nodes is kept constant through the computing process but the nodes are allowed to move dynamically based on some pre-defined criteria (See [9] and references therein).
- **p-refinement:** the nodes and the number of nodes are both fixed but the accuracy can be improved by utilizing higher-order terms in the approximating Taylor series expansion (See [32] and references therein).
- **m-refinement:** the computational mesh is completely rebuilt regarding to error indicator introduced from discretization step (See [33] and references therein).

The refinement scheme proposed in this work is fallen into the h-refinement category. The following adaptation ingredients are a further developed version of the work of Kaennakham and Chuathong [31], being proposed here in this work aiming to cooperate numerically with RPIM for modelling the convection-dominated phenomena.

2.2.1. The Proposed Means of Error Indicator. The node adaptation proposed in this work is proceeded based on the local change of the chosen physical parameter, the 'Péclet number (Pe)' which is the ratio of the contributions to mass transport by convection to those by diffusion, expressed for a node $\left(x_{i,} y_{j}\right) := (i, j)$ as follows;

$$\mathrm{Pe}_{(i,j)} = \frac{L \left\| \mathbf{U}_{(i,j)} \right\|}{D} = \frac{\textit{Local Convection Rate}}{\textit{Local Diffusion Rate}} \tag{2.12}$$

Where L is a characteristic length scale defined locally as the distance of the node (i, j) to the nearest node around itself, $\left\| \mathbf{U}_{(i,j)} \right\|$ is the local velocity magnitude, and D is the characteristic diffusion coefficient, and $j = 1, 2, ..., N$. Numerically, this local change can be tracked using the following formulas.

$$\left(\mathrm{Pe}_{(i,j)}\right)_x = \left| \frac{\mathrm{Pe}_{(i+1,j)} - 2\mathrm{Pe}_{(i,j)} + \mathrm{Pe}_{(i-1,j)}}{\left(x_{i+1} - x_i\right)\left(x_i - x_{i-1}\right)} \right|, \left(\mathrm{Pe}_{(i,j)}\right)_y = \left| \frac{\mathrm{Pe}_{(i,j+1)} - 2\mathrm{Pe}_{(i,j)} + \mathrm{Pe}_{(i,j-1)}}{\left(y_{i+1} - y_i\right)\left(y_i - y_{i-1}\right)} \right| \tag{2.13}$$

Then the *error indicator* used to drive the node adaptation algorithm, $\xi^{(k)}$, is obtained for a k^{th} -node as follows;

$$\xi_{\mathrm{A}}^{(k)} = \left(\Delta_{cell}^{(k)}\right)^{w} \sqrt{\frac{\left[\left(\mathrm{Pe}^{(k)}\right)_y\right]^2 + \left[\left(\mathrm{Pe}^{(k)}\right)_x\right]^2}{2}} \tag{2.14}$$

Where $\Delta_{cell}^{(k)} = \Delta x^{(k)} \Delta y^{(k)} \approx 4(h_x^{(k)})(h_y^{(k)}) \approx \frac{Characteristic\ Domain\ Lenght}{\sqrt{The\ total\ number\ of\ nodes}}$, the volume weight $w = 1$ and $|\cdot|$ is the absolute value. In order to prevent the algorithm from producing a strong change of the raw values of the refinement variable during the computation, a means of normalization is needed and for this task the *normalized error indicator,* $\Lambda_{(i,j)}$, is defined as;

$$\Lambda_{(i,j)} = \frac{\xi_{(i,j)}}{\max\{\xi_{(l,k)}\}} \tag{2.15}$$

So that $0 < \Lambda_{(i,j)} \leq 1$. With a pre-defined lower threshold, θ_{low} , and upper threshold, θ_{up} , where $0 < \theta_{low} < \theta_{up} < 1$, the computational domain is divided into 3 sub-areas;

- Refinement areas : those nodes with $\Lambda_{(i,j)} > \theta_{up}$
- Coarsen areas : those nodes with $\Lambda_{(i,j)} < \theta_{low}$
- Intact areas : those nodes with $\theta_{low} \leq \Lambda_{(i,j)} \leq \theta_{up}$

2.2.2. Node Adaptive Manner. Figure 2 illustrates the proposed node adaptation manner where a node is marked to be adapted. Four child-nodes are then created amongst their three neighbours in a centroid manner. With this centroid-line node generator, it can ensure that no child-nodes generated by neighbouring parents shall be overlapped. This is called 'one-level of refinement' and the coarsen process is simply done by the opposite direction, i.e. from (c) to (a) whereas the initial or parent node cannot be removed.

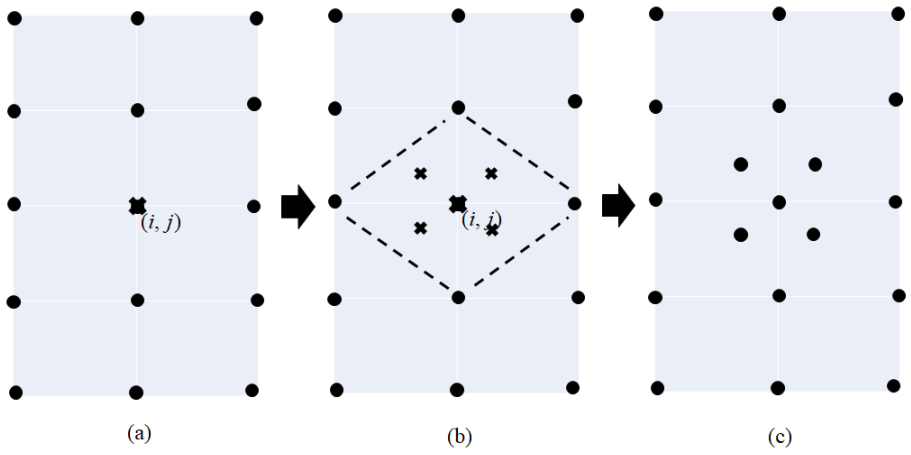

Figure 2. One-level of node-adaptation manner with one parent-node and four child-nodes.

3. Implementation of RPIM for Steady Convection-Dominated PDE

To study the physical phenomena of the system when the convection force is dominant, a benchmark 2D steady state of convection-diffusion problem [4] is focused on. The governing equation is as

follows;

$$L(u)=\mathbf{V}^T\cdot\nabla u-\nabla^T(\mathbf{D}\nabla u)+\beta u-q(\mathbf{x})=0 \tag{3.1}$$

The problem domain is $(x,y)\in\Omega=[0,1]\times[0,1]$, and the coefficients are $\mathbf{D}=\begin{bmatrix}\eta_x & 0\\ 0 & \eta_y\end{bmatrix}$, $\mathbf{V}=\left[V_x,V_y\right]=[3-x,4-y]$, and $\beta=1$ in which $\eta_y=\eta_y=\eta$ is a given constant of diffusion coefficient. The boundary condition is considered as $u(0,y)=u(1,y)=u(x,0)=u(x,1)=0$.

The exact solutions for this problem is given by;

$$u^{exact}=\sin(x)\left(1-\exp\left(-\frac{2(1-x)}{\eta_x}\right)\right)y^2\left(1-\exp\left(-\frac{3(1-y)}{\eta_y}\right)\right) \tag{3.2}$$

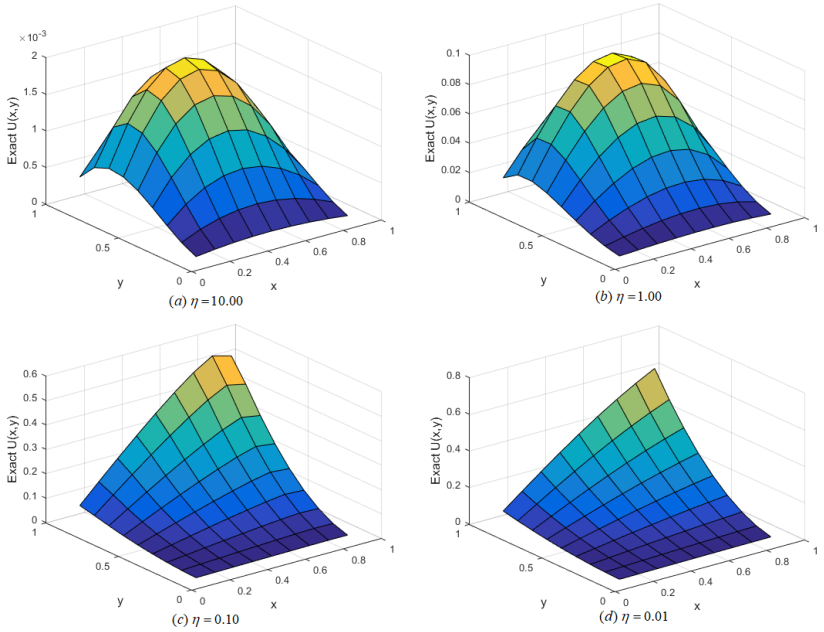

Figure 3. Solution profiles for different stages of diffusion-force domination.

Equation (2.4) and constrain equation (2.6) are applied to the governing equation and in this work, $M=6$ is needed to be imposed in order to obtain the coefficient matrices $[\bar{\mathbf{a}}]$.

With N being the number of centres, this leads to the following matrix equation form.

$$\frac{1}{\eta}\left[\mathbf{g}_{dig}\right]+\left[\mathbf{A}\quad\mathbf{C}\right]=\frac{1}{\eta}\left(\left[\left(\mathbf{V}_x\right)_{dig}\right]\left[\mathbf{R}^x\quad\mathbf{P}^x\right]-\left[\left(\mathbf{V}_y\right)_{dig}\right]\left[\mathbf{R}^y\quad\mathbf{P}^y\right]+\beta\left[\mathbf{u}_{dig}\right]\right)[\bar{\mathbf{a}}] \tag{3.3}$$

For $i=1,2,...,N$ and with the following matrices;

$$[\mathbf{A}]=\begin{bmatrix}\left(R^{xx}+R^{yy}\right)_{11} & \left(R^{xx}+R^{yy}\right)_{12} & \cdots & \left(R^{xx}+R^{yy}\right)_{1N}\\ \left(R^{xx}+R^{yy}\right)_{21} & \left(R^{xx}+R^{yy}\right)_{22} & \cdots & \left(R^{xx}+R^{yy}\right)_{2N}\\ \vdots & \vdots & \ddots & \vdots\\ \left(R^{xx}+R^{yy}\right)_{N1} & \left(R^{xx}+R^{yy}\right)_{N2} & \ldots & \left(R^{xx}+R^{yy}\right)_{NN}\end{bmatrix}_{N\times N},\left(\mathbf{V}_x\right)_{dig}=\begin{bmatrix}\left(V_x\right)_1 & 0 & 0 & 0\\ 0 & \left(V_x\right)_2 & 0 & 0\\ 0 & 0 & \ddots & 0\\ 0 & 0 & 0 & \left(V_x\right)_N\end{bmatrix}_{N\times N},$$

$$[\mathbf{C}]=\begin{bmatrix}\left(P^{xx}+P^{yy}\right)_{11} & \left(P^{xx}+P^{yy}\right)_{12} & \cdots & \left(P^{xx}+P^{yy}\right)_{1M}\\ \left(P^{xx}+P^{yy}\right)_{21} & \left(P^{xx}+P^{yy}\right)_{22} & \cdots & \left(P^{xx}+P^{yy}\right)_{2M}\\ \vdots & \vdots & \ddots & \vdots\\ \left(P^{xx}+P^{yy}\right)_{N1} & \left(P^{xx}+P^{yy}\right)_{N2} & \ldots & \left(P^{xx}+P^{yy}\right)_{NM}\end{bmatrix}_{N\times M},\left(\mathbf{V}_y\right)_{dig}=\begin{bmatrix}\left(V_y\right)_1 & 0 & 0 & 0\\ 0 & \left(V_y\right)_2 & 0 & 0\\ 0 & 0 & \ddots & 0\\ 0 & 0 & 0 & \left(V_y\right)_N\end{bmatrix}_{N\times N}$$

$$\left[\mathbf{u}_{dig}\right]=\begin{bmatrix}u_1 & 0 & 0 & 0\\ 0 & u_2 & 0 & 0\\ 0 & 0 & \ddots & 0\\ 0 & 0 & 0 & u_N\end{bmatrix}_{N\times N},\qquad \left[\mathbf{g}_{dig}\right]=\begin{bmatrix}g_1 & 0 & 0 & 0\\ 0 & g_2 & 0 & 0\\ 0 & 0 & \ddots & 0\\ 0 & 0 & 0 & g_N\end{bmatrix}_{N\times N},$$

$$[\bar{\mathbf{a}}]=\begin{bmatrix}(a_1)_1 & (a_1)_2 & \ldots & (a)_N & (a_2)_1 & (a_2)_2 & (a_2)_3 & \ldots & (a_2)_M\end{bmatrix}^T.$$

Where $\left(R^{xx}+R^{yy}\right)=\left(\frac{\partial^2}{\partial x^2}+\frac{\partial^2}{\partial y^2}\right)R(r)$.

With the polynomial constrains, this leads to a transformation of equation above into a new system of equations where the solutions exist and are mathematically unique, and are expressed as follows;

$$\frac{1}{\eta}\left[\mathbf{g}_{dig}\right]+[\mathbf{A}\quad\mathbf{C}]=\frac{1}{\eta}\left(\left[\left(\mathbf{V}_x\right)_{dig}\right]\left[\mathbf{R}^x\quad\mathbf{P}^x\right]-\left[\left(\mathbf{V}_y\right)_{dig}\right]\left[\mathbf{R}^y\quad\mathbf{P}^y\right]+\beta\left[\mathbf{U}_{dig}\right]\right)[\bar{\mathbf{a}}] \tag{3.4}$$

Thus, for a $k^{th}-$ iteration, the coefficient matrix $\left[\bar{\mathbf{a}}^{(k)}\right]$ can be achieved by;

$$\left[\bar{\mathbf{a}}^{(k)}\right]=\left[\boldsymbol{\Xi}^{(k-1)}\right]^{-1}\left[\boldsymbol{\Psi}^{(k-1)}\right] \tag{3.5}$$

Where;

$$\left[\boldsymbol{\Xi}^{(k-1)}\right]=\frac{1}{\eta}\left(\left[\left(\mathbf{V}_x\right)_{dig}\right]\left[\mathbf{R}^x\quad\mathbf{P}^x\right]-\left[\left(\mathbf{V}_y\right)_{dig}\right]\left[\mathbf{R}^y\quad\mathbf{P}^y\right]+\beta\left[\mathbf{U}_{dig}^{(k-1)}\right]\right) \tag{3.6}$$

and

$$\left[\boldsymbol{\Psi}^{(k-1)}\right]=\frac{1}{\eta}\left[\mathbf{g}_{dig}\right]+\left[\mathbf{A}^{(k-1)}\quad\mathbf{C}^{(k-1)}\right] \tag{3.7}$$

Note that with $k=1$, then $\mathbf{U}^{(k-1)}$ is the initial "guess" value of $\mathbf{U}$.

4. Numerical Experiments and General Discussion

Since all the RBFs under this investigation contain the shape ε , choosing an adequate one for each simulation is firstly to be reasoned. In the past, some attempts to pinpoint the optimal value of ε involve the classic work of Hardy [34] where it was shown that by fixing the shape at $\varepsilon = 1/(0.815d)$, where $d = (1/N)\sum_{i=1}^{N} d_i$, and d_i is the distance from the node to its nearest neighbour, good results should be anticipated. Franke and Schaback [35] concluded that the choice of a fixed shape of the form $\varepsilon = 0.8\sqrt{N}/D$ with D being the diameter of the smallest circle containing all data nodes, can also be a good alternative. In 2000, Zhang et al. [36] demonstrated and concluded that the optimal shape parameter is highly problem dependent. In 2002, Wang and Lui [37] pointed out that by analysing the condition number of the collocation matrix, a suitable range of derivable values of ε can be found. Later in 2003, Lee et al. [38] suggested that the final numerical solutions obtained are found to be less affected by the method when the approximation is applied locally rather than globally. A rather recent work is the selection of an interval for variable shape parameter by Biazar and Hosami in 2016 [39], where a novel algorithm for determining and interval was proposed. To sum up, finding an optimal choice of this parameter is highly problem dependent. For this reason, all best shapes shown in this work were obtained purely by carrying out a large number of experiments under different constraints and conditions for each simulation and observing the trends in errors produced.

4.1. Error Measurement Norms

All numerical solutions obtained from the whole study are validated by comparing against the analytical solutions using different types of error norms as listed in Table 1, or some other numerical works where available in literature.

Table 1. Error Norms adopted in this work.

Error Norm	Symbol Defined	Mathematical Formula
Maximum	L_∞	$\max_{1\le i\le N}\left\|u^{ext.}(\mathbf{x}_i)-u^{appx.}(\mathbf{x}_i)\right\|$
Root-Mean-Square	L_{RMS}	$\left(\frac{1}{N}\sum_{j=1}^{N}\left(u^{ext.}(\mathbf{x}_i)-u^{appx.}(\mathbf{x}_i)\right)^2\right)^{1/2}$
Absolute	L_{Abs}	$\left\|u^{ext.}(\mathbf{x}_i)-u^{appx.}(\mathbf{x}_i)\right\|$
Relative	L_{Rlv}	$\left\|\frac{u^{ext.}(\mathbf{x}_i)-u^{appx.}(\mathbf{x}_i)}{u^{ext.}(\mathbf{x}_i)}\right\|$
Root-Relative-Square	L_{RRS}	$\left[\frac{\sum_{i=1}^{N}\left(u^{ext.}(\mathbf{x}_i)-u^{appx.}(\mathbf{x}_i)\right)^2}{\sum_{i=1}^{N}\left(u^{ext.}(\mathbf{x}_i)\right)^2}\right]^{1/2}$

All computing experiments were carried out on the same computer; Intel(R) Core(TM) i7-5500U CPU @ 2.40GHz with 8.00 GB of RAM and 64-bit Operating System.

4.2. Method Validation Via. Interpolation Problem

The first numerical experiment shall be dedicated to validating the methodology of RPIM with an interpolation problem. The interpolation problem starts with a set of discrete data $\mathbf{X}=\{\mathbf{x}_i\}_{i=1}^{N}, \mathbf{x}_i \in \mathbb{R}^{\mathrm{d}}$ where for each $\mathbf{x}_i$ there is its corresponding real value $y_i \in \mathbb{R}$, then the task is to construct a continuous function $\Phi(\mathrm{x}):\mathbb{R}^{\mathrm{d}} \to \mathbb{R}$ such that;

$$\Phi(\mathbf{x}_i) = y_i \tag{4.1}$$

For all $i=1,2,...,N$. The first validation of the scheme proposed in this work is done using a benchmark Franke-type function [40], defined on a unit square-domain as follows.

$$\begin{aligned} f(x,y) = {} & 0.75\exp\left[-\frac{(9x-2)^2}{4}-\frac{(9y-2)^2}{4}\right]+0.75\exp\left[-\frac{(9x+1)^2}{49}-\frac{(9y+1)}{10}\right] \\ & +0.5\exp\left[-\frac{(9x-7)^2}{4}-\frac{(9y-3)^2}{4}\right]-0.2\exp\left[-(9x-4)^2-(9y-7)^2\right] \end{aligned} \tag{4.2}$$

As regarded as one of the most influential factors (ε), the shape parameter is firstly investigated. L_∞ errors produced by using each type of RBF at a wide range value of ε are shown in Figure. 4 (left). For this interpolation problem, it is found that all types of RBF reveal comparatively good result accuracy when $\varepsilon \in (1.9, 2.1)$. Beyond this point, it is interesting to see that GA, IQ, and IMQ start to lose their accuracy where even better solutions are still obtainable for CMT and MQ. For MQ-RBF **(**at $\varepsilon = 8.00$) in particular, the error is found to as low as $3.12E-03$ and the corresponding numerical solutions are plotted in Figure 4 (right).

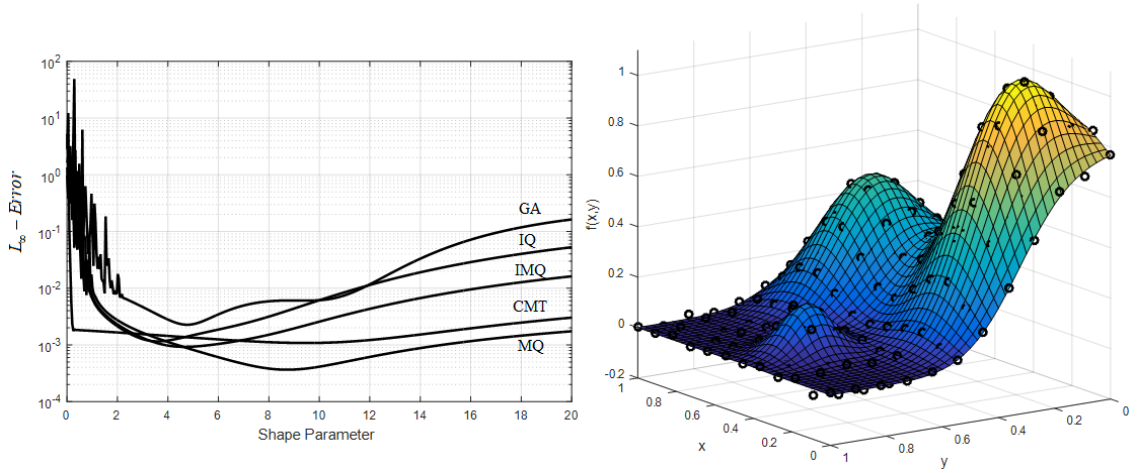

Figure 4. Left) L_∞ error measured with the change of shape parameter $0.001 \le \varepsilon \le 20.00$, and Right) Exact solution profile with black dots representing those computed by MQ-RBF ($\varepsilon = 8.00$) .

Table 2: L_{Abs} and L_{Rlv} measured at selected centres obtained from all RBFs compared with the exacts when using the same shape of $\varepsilon = 4.25$.

(x,y)	GA		IMQ		MQ		CMT		IQ	
	L_{Abs}	L_{Rlv}	L_{Abs}	L_{Rlv}	L_{Abs}	L_{Rlv}	L_{Abs}	L_{Rlv}	L_{Abs}	L_{Rlv}
(0.00,0.81)	2.49E-04	2.82E-01	1.01E-04	1.14E-01	9.92E-05	1.13E-01	1.97E-04	2.24E-01	5.01E-05	5.69E-02
(0.09,0.45)	9.82E-05	4.27E-04	4.62E-04	2.01E-03	6.56E-05	2.85E-04	3.35E-05	1.46E-04	4.62E-04	2.01E-03
(0.36,0.45)	4.25E-04	1.95E-03	5.20E-04	2.39E-03	3.58E-04	1.64E-03	2.82E-04	1.29E-03	5.45E-04	2.50E-03
(0.45,0.36)	1.84E-03	6.17E-03	9.84E-04	3.30E-03	1.06E-03	3.57E-03	6.67E-04	2.24E-03	1.01E-03	3.41E-03
(0.45,0.45)	6.54E-04	4.03E-03	4.49E-04	2.77E-03	5.88E-04	3.63E-03	3.95E-04	2.43E-03	4.12E-04	2.54E-03
(0.90,0.00)	2.39E-04	1.50E-03	1.91E-04	1.20E-03	2.10E-04	1.32E-03	2.11E-05	1.33E-04	1.72E-04	1.08E-03
(0.90,0.09)	4.75E-04	2.33E-03	2.89E-04	1.42E-03	1.53E-04	7.49E-04	2.54E-04	1.25E-03	9.41E-05	4.62E-04
(0.90,0.27)	2.02E-04	5.48E-04	3.30E-04	8.96E-04	3.24E-04	8.80E-04	2.39E-04	6.50E-04	3.80E-04	1.03E-03
(1.00,0.27)	8.57E-05	4.28E-04	1.10E-04	5.51E-04	8.32E-05	4.15E-04	1.95E-04	9.73E-04	7.70E-06	3.84E-05

4.3. Node-Adaptation Scheme with Non-rectangular domain

In this second test case, the Poisson equation shown below is numerically solved by RPIM with and without the use of the proposed node-adaptation algorithm.

$$\nabla^2 u = \left(\frac{\partial^2}{\partial x^2} + \frac{\partial^2}{\partial y^2} \right) u = -x^2 \tag{4.3}$$

This is defined on the domain with an elliptical boundary expressed as $\left(x^2/4\right) + y^2 = 1$. Where the boundary condition is taken directly from the exact solution which is expressed as follows;

$$u(x,y) = -\frac{1}{246}\left(50x^2 - 8y^2 + 33.6\right)\left(\frac{x^4}{4} + y^2 - 1\right) \tag{4.4}$$

In this case the number of nodes on the domain boundary is kept intact. Errors produced by each RBF under this example are shown in Table 3 and it can be seen that reasonable agreement in solution accuracy can be obtained for all types of RBFs. In this table, solution numerically computed with and without using the proposed node adaptation are compared against each other. Based on both error norms used, IMQ, is seen to slightly outperform the others with the lowest L_{RMS} of 2.726 E -04 when using node-adaptation scheme and of 1.502E-04 without node-adaptation scheme. In terms of CPU-time needed, all RBFs under the use of adaptation method show promising aspects when compared with those obtained using the fixed-node cases. The lowest amount of CPU-time involved is found under the case of CMT-RBF (1.729s.) and the highest is found for GA-RBF (2.225s.). The final number of nodes produced by the algorithm, noted as $FNd.$, is clearly seen to dramatically reduced by 68% at most when using CMT-RBF where only 49 extra nodes are generated from 51 original nodes in order to reach the same level of accuracy as that of fixed-node case, shown in Figure 5. This aspect confirms the advantage of the node-algorithm scheme proposed in this work.

Table 3: Error norms with CPU-time and final number of nodes produced, $FNd.$ and the same shape of $\varepsilon = 0.1$. With (using 51 initial nodes), and Without using the node-adaptive algorithm.

RBF	L_{RMS}		L_{∞}		CPU-time (s)		$FNd.$	
	With	Without	With	Without	With	Without	With	Without
GA	2.825E-03	1.921E-04	8.690E-03	4.251E-03	2.225	3.841	116	315
IMQ	2.726E-04	1.502E-04	1.074E-03	3.058E-04	1.914	3.991	108	315
MQ	1.669E-03	2.025E-04	7.276E-03	1.255E-03	1.884	4.012	116	315
CMT	1.003E-02	2.001E-04	3.638E-02	5.011E-04	1.729	4.174	100	315
IQ	3.824E-04	1.884E-04	1.667E-03	6.225E-04	2.120	3.705	104	315

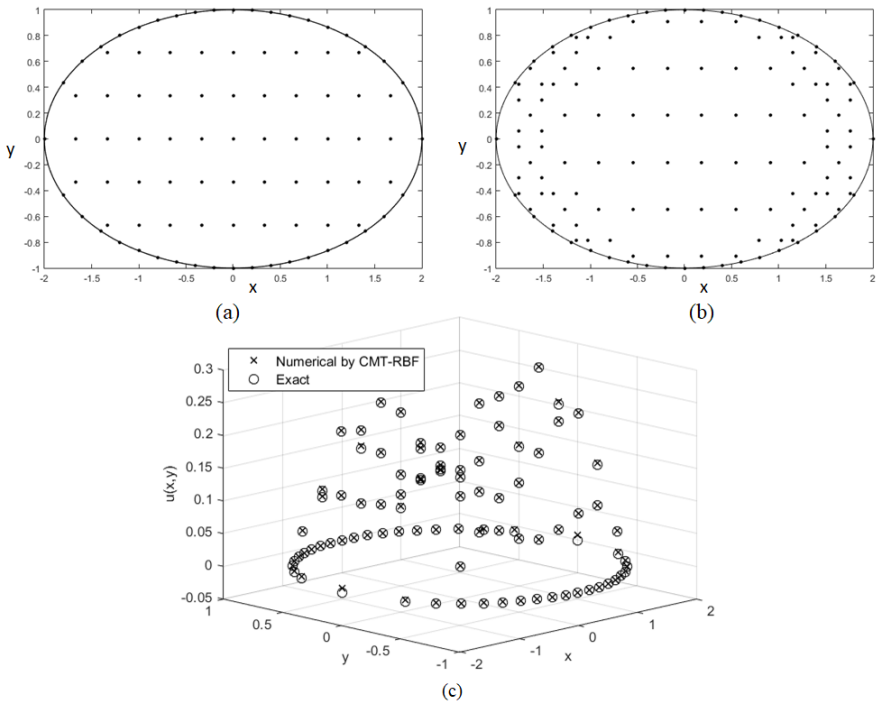

Figure 5. Results obtained with $\varepsilon = 0.1$, $\left(\theta_{lower}, \theta_{upper}\right) = \left(0.1, 0.5\right)$; (a) Initial node distribution, (b) Final node distribution after using the node-adaptive algorithm in conjunction with CMT-RBF, and (c) Solution comparison at selected centres.

4.4. Convection-Dominated Phenomena Simulation

In Section 3, one of the benchmark cases of convection-dominated equation is numerically derived via. the method of RPIM. It is pointed out that the diffusion coefficient, η, plays a crucial role in determining the level of convective force in the system. One numerical experiment that is well-known and nicely documented is that by Gu & Liu [4] where the main results at different η (measured by L_{RRS}) are listed in Table 4. With a fixed interval of refinement threshold of $\left(\theta_{lower}, \theta_{upper}\right) = \left(0.5, 0.8\right)$, numerical solutions computed by each type of RBF are also shown in the same table, together with their corresponding optimal shape, ε_{opt} , and the final number of nodes generated, FNd.

Table 4: Measurement of L_{RRS} at different η obtained from using each RBF type (with their optimal shape parameter and final number of nodes, ε_{opl} / $FNd.$) simulated using $\left(\theta_{lower},\theta_{upper}\right)=\left(0.5,0.8\right)$ with 100 initial nodes.

η	Gu & Liu [Gu and Liu (2006)].	GA (ε_{opl} / $FNd.$)	IMQ (ε_{opl} / $FNd.$)	MQ (ε_{opl} / $FNd.$)	CMT (ε_{opl} / $FNd.$)	IQ (ε_{opl} / $FNd.$)	Fixed-Node with MQ
100	0.2450	0.0050 (1.0/305)	0.0381 (0.25/297)	0.1526 (0.1/201)	0.0035 (1.0/305)	0.0053 (1.0/305)	0.8153 (1.5/144)
10	0.2550	0.9930 (30/181)	0.0004 (0.50/291)	0.0068 (0.25/287)	0.0172 (5.0/305)	0.0172 (1.50/296)	1.1223 (9.0/144)
1	0.3460	0.9968 (50/160)	0.0033 (0.70/223)	0.0014 (0.5/223)	0.1172 (10/245)	0.0697 (5.0/233)	6.5153 (18.5/144)
0.1	1.2760	0.9891 (55/125)	0.0936 (0.65/130)	0.2421 (0.5/123)	0.4568 (12/130)	0.1432 (10.0/125)	11.1057 (11.0/400)
0.01	15.8320	0.9239 (65/126)	0.1900 (15.0/145)	0.4487 (10.0/142)	0.6899 (17/122)	0.2858 (15.0/118)	64.6012 (14.5/400)
0.001	195.3450	1.6891 (100/126)	0.2875 (20.0/163)	0.5481 (15.0/186)	0.9502 (20/245)	0.2582 (19.0/147)	315.2515 (10.4/400)

At moderate-high convection phenomena, $1\le\eta\le100$, it is seen from the table that all RBFs are able to produce reasonable results quality. MQ-RBF, in particular, when the problem becomes more convective, in conjunction with the node-adaptation scheme, it reveals the lowest value of error of 0.0014 with $\varepsilon_{opl}=0.5$ and $FNd.=223$. In terms of the number of nodes involved, nevertheless, the small number of nodes of 160 are found for GA-RBF with L_{RRS} = 0.9968. When the situation becomes even more convective-dominated, $100\le\eta\le0.001$, as expected, all cases are found to lose their accuracy. Nevertheless, it should be noticed that those solutions obtained using node-adaptation remain significantly lower than those presented in the work of Gu & Liu [4].

At even higher convective-dominated ($\eta=5.0E-03$ **)**, which has not been documented formerly in literature, Figure 6 illustrates the node distribution obtained from using each RBF with the node-adaptation scheme. All cases were run based on $\left(\theta_{lower},\theta_{upper}\right)=\left(0.4,0.7\right)$ and it can be observed to provide highly promising aspects both in terms of accuracy (with $L_{RRS}\le1.00E+10.00$) and the number of nodes required ($FNd.<200$). The best case revealed from this final experiment is that using IMQ-RBF where the error is as low as 0.8812 with only 141 nodes being generated and computed on.

For comparison purposes, simulations by RPIM with MQ-RBF based on a fixed number of uniformly distributed nodes were also parallelly investigated for all levels of convective-force domination and the results are declared in Table 4. It is clearly seen that the solutions are comparatively worse in all cases particularly at the very highly convective-dominated stage, η = 0.001, with L_{RRS} =315.2515 where up to 400 nodes were needed. With the use of the convectional collocation method as applied in [4], the error is found to reach up to 195.34, approximately 757 times higher than the node-adaption IQ-RBF. This strongly confirms the benefit and promising aspect of using the proposed node-adaptive algorithm used in conjunction with RPIM.

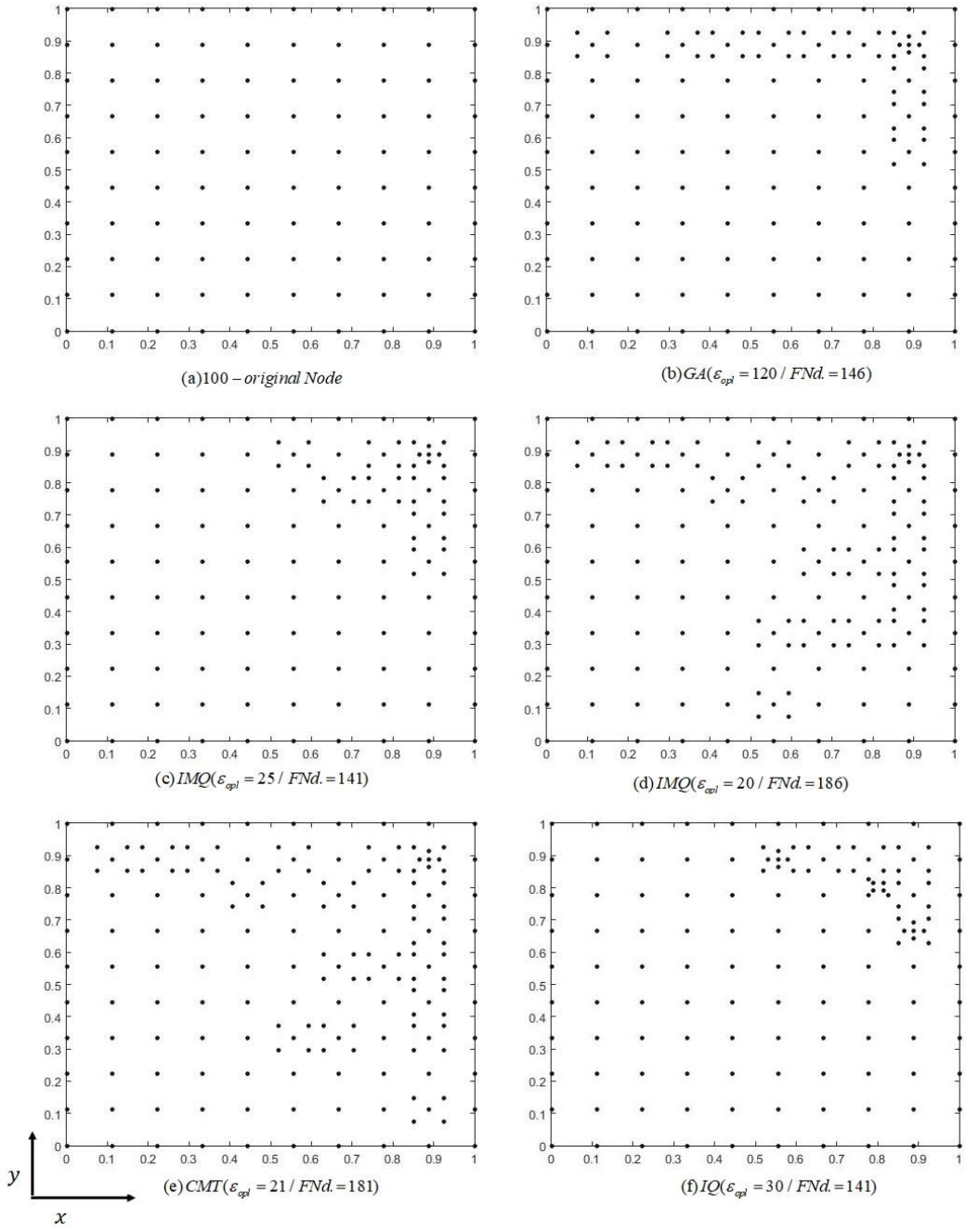

Figure 6. Node distribution of each RBF (with the optimal shape $,\varepsilon_{opl},$ and the final node number $FNd.,$) after performing the node-adaption algorithm at $\eta = 5.0E-03$ using $\left(\theta_{lower},\theta_{upper}\right)=\left(0.4,0.7\right)$ and 10×10 initial nodes.

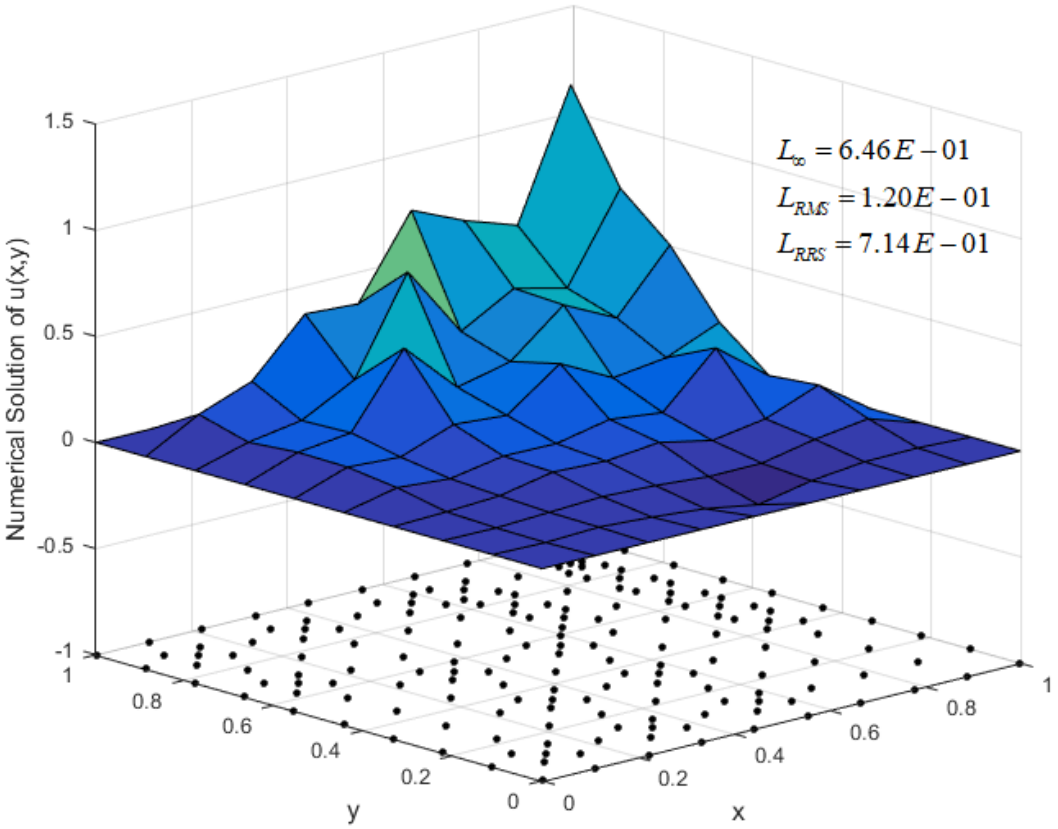

Figure 7. Solution profile simulated using CMT-RBF with 100 initial nodes obtained for $\eta = 1.00E-03$, $(\theta_{lower}, \theta_{upper}) = (0.5, 0.8)$ with the optimal shape $\varepsilon_{opl} = 45.00$ and the final nodes number after adaptation is $FNd. = 182$.

Figure 7 displays the solution profile obtained at very high value of convection force, where no other numerical works available in literature yet. At this stage, simulations when using a fixed-node with 35×35 nodes were also investigated and the results are $L_\infty = 1321.25$, $L_{RMS} = 365.61$, and $L_{RRS} = 805.74$. With this information, it can then be clearly seen that the proposed node-adaptation algorithm is able to produce a significant improvement in terms of both accuracy and the number of computational nodes involved. It has to also be noticed that the potential layers anticipated to take place along the edges $x = 1$ and $y = 1$ are treated with no extra treatments. Instead, the algorithm applied in conjunction with this type of collocation method taking place all over the domain is able to pick up well the phenomena occurring along those edges.

5. Conclusion

In this work a node-adaptation scheme is proposed and used in conjunction with the radial point interpolation meshfree method. Five popular choices of radial basis (RBF) functions are also under investigation; Multiquadric (MQ), Gaussian (GA), Inverse Quadratic (IQ), and Cubic Matern (CMT). The combination of these numerical treatments is applied to solve the problem with strong convection force in steady state. The investigation began with studying the effect of the RBF shape parameter by adopting a benchmark case of interpolation called 'Franke' function before moving on more

complicated PDEs. Several error measuring schemes were adopted to monitor the effectiveness of the proposed method in overall. It is found that with having the local problem parameter as the refinement, the use of the proposed node-adaptation method leads to a reduction in both CPU-time and storage in computation process. Moreover, solution improvements are noticeable for all RBFs under investigation. This promising aspect becomes even more obvious when fixed-node cases are found to significantly lose their capability to capture the problem phenomena when convection becomes dominant. Another benefit gained from using the node-adaptation discovered is that all RBFs tend to be less sensitive to their shape parameter making it much easier and more reliable, requiring less human judgement during the computational process. Nevertheless, it is still great of challenge to further improve the adaptation scheme towards more complex problems and this remains our future work.

Acknowledgement

The authors would like to express our sincere appreciation to the Centre of Excellence in Mathematics, Thailand, for their kind support.

Conflicts of Interest: The authors declare that there are no conflicts of interest regarding the publication of this paper.

References

[1] Djidjeli K, Chinchapatnam P P, Nair P B and Price W G 2004 Global and Compact Meshless Schemes for the Unsteady Convection–Diffusion Equation *International Symposium on Health Care and Biomedical Research Interaction* 1-8

[2] Morton K W 1996 *Numerical Solution of Convection-Diffusion Problems,* Chapman and Hall, London

[3] Lin H and Atluri S N 2000 Meshless Local Petrov-Galerkin (MLPG) Method for Convection-Diffusion Problems *Comput. Model. Eng. Sci.* **1** 45-60

[4] Gu Y T and Liu G R 2006 Meshless Techniques for Convection Dominated Problems *Comput. Mech.* **38** 171-82

[5] Zhang S H and Wang W Q 2010 A Stencil of the Finite–Difference Method for the 2D Convection Diffusion Equation and its New Iterative Scheme *Int. J. Comput. Math.* **87** 2588-2600

[6] Kaennakham S and Chuathong N 2017 Solution to a Convection-Diffusion Problem Using a New Variable Inverse-Multiquadric Parameter in a Collocation Meshfree Scheme *Int. Jnl. of Multiphysics* **11** 359-74

[7] Chanthawara K, Kaennakham S and Toutip W, 2016 Numerical Study and Comparison of Radial Basis Functions in Applications of the Dual Reciprocity Boundary Element Method to Convection-Diffusion Problems *Progress in Applied Mathematics in Sciences and Engineering*, *AIP Conference Proceedings **1705** 020029*

[8] Deng Y, Liu C, Peng M and Cheng Y 2015 The Interpolating Complex Variable Element-Free Galerkin Method for Temperature Field Problems *Int. J. Appl. Mech.* **7** 1550017

[9] Cao W, Huang W H and Russell R D 2001 An Error Indicator Monitor Function for an r-Adaptive Finite Element Method *J. Comput. Phys*. **170** 871-92

[10] Sheu G Y 2013 Prediction of Probabilistic Settlements by the Perturbation-Based Spectral Stochastic Meshless Local Petrov–Galerkin Method *Geotech. Geol. Eng.* **31** 1453-64

[11] Dai B, Zheng B, Liang Q and Wang L 2013 Numerical Solution of Transient Heat Conduction Problems Using Improved Meshless Local Petrov–Galerkin Method *Appl. Math. Comput.* **219** 10044-52

[12] Gao H and Wei G 2016 Complex Variable Meshless Manifold Method for Elastic Dynamic Problems *Math. Probl. Eng.* **2016** 1-8

[13] Kansa E J 1990 Multiquadrics—A Scattered Data Approximation Scheme with Applications to Computational Fluid-Dynamics—II Solutions to Parabolic, Hyperbolic and Elliptic Partial Differential Equations *Comput. Math. Appl.* **19** 147-61
[14] Chandhini G S and Sanasiraju Y V S S 2007 Local RBF-FD Solutions for Steady Convection-Diffusion Problems *Int. J. Numer. Methods Eng.* **72** 352-78
[15] Wen P H and Hon Y C 2007 Geometrically Nonlinear Analysis of Reissner-Mindlin Plate by Meshless Computation *Comput. Model. Eng. Sci.* **21** 177-92
[16] Al-Gahtani H J and Naffa M 2009 RBF Meshless Method for Large Deflection of Thin Plates with Immovable Edges *Eng. Anal. Bound. Elem.* 33 176-83
[17] Ferreira A J M, Roque C M C and Martins P A L S 2004 Radial Basis Functions and Higher-Order Shear Deformation Theories in the Analysis of Laminated Composite Beams and Plates *Compos. Struct.* **66** 287-93
[18] Liu Y, Liew K M, Hon Y C and Zhang X 2005 Numerical Simulation and Analysis of an Electroactuated Beam using Radial Basis Function *Smart. Mater. Struct.* **14** 1163-71
[19] Wang J G and Liu G R 2002 A Point Interpolation Meshless Method Based on Radial Basis Functions *Int. J. Numer. Meth.Eng.* **54** 1623-48
[20] Liu X, Liu G R, Tai K and Lam K Y 2002 Radial Basis Point Interpolation Collocation Methodfor 2-D Solid Problem *Advances in Meshfree and X-FEM Methods* **2** 35-40
[21] Bozkurt O Y, Kanber B and Asik M Z 2013 Assessment of RPIM Shape Parameters for Solution Accuracy of 2D Geometrically Nonlinear Problems *Int. J. Comput. Methods* **10** 1350003
[22] Ghaffarzadeh H, Barghian M, Mansouri A and Sadeghi M H 2016 Study on Meshfree Hermite Radial Point Interpolation Method for Flexural Wave Propagation Modeling and Damage Quantification *Lat. Am. J. Solids. Stru.* **13** 2606-27
[23] Ma J, Wei G, Liu D and Liu G 2017 The Numerical Analysis of Piezoelectric Ceramics Based on the Hermite-Type RPIM *Appl. Math. Comput.* **309** 170-82
[24] Lazzaro D and Montedusco L B 2002 Radial Basis Functions for the Multivariate Interpolation of Large Scattered Data Sets *J. Comput. Appl. Math.* **140** 521-36
[25] Yao G 2010 *Local Radial Basis Function Methods for Solving Partial Differential Equations* (United Stated: The University of Southern Mississippi)
[26] Kaennakham S, Holdø A E and Lambert C 2010 A New Simple H-Mesh Adaptation Algorithm for Standard Smagorinsky LES: a First Step of Taylor Scale as a Refinement Variable *Int. Jnl. of Multiphysics* **4** 33-50
[27] Libre N A, Emdadi A, Kansa E J and Shekarchi M 2008 A Fast Adaptive Wavelet Scheme in RBF Collocation for Nearly Singular Potential PDEs *Comput. Model. Eng. Sci.* **38** 263-84
[28] Bertrand A and Moonen M 2010 Distributed Adaptive Node–Specific Signal Estimation in Fully Connected Sensor Networks–Part II: Simultaneous and Asynchronous Node Updating *IEEE Transaction on Signal Processing* **58** 5292-306
[29] Ling L 2012 An Adaptive–Hybrid Meshfree Approximation Method *Int. J. Numer. Meth. Eng.* **89** 637-57
[30] Biazar J and Hosami M 2015 Redistribution of Nodes with Two Constraints in Meshless Method of Line to Time-Dependent Partial Differential Equations *Int. J. Differ. Equ.* **2015** 1-8
[31] Kaennakham S and Chuathong N 2019 An Automatic Node-Adaptive Scheme Applied with a RBF-Collocation Meshless Method *Appl. Math. Comput.* **348** 102-25
[32] Zienkiewicz O C and Zhu J Z 1987 A Simple Error Estimator and Adaptive Procedure for Practical Engineering Analysis *Int. J. Numer. Meth. Eng.* **24** 337-57
[33] Hetu J F and Pelletier D H 1992 Fast, Adaptive Finite Element Scheme for Viscous Incompressible Flows *AIAA Journal* **30** 403-11
[34] Hardy R L 1971 Multiquadric Equations of Topography and Other Irregular Surfaces *J. Geophys. Res. Atmos.* **76** 1905-15

[35] Franke C and Schaback R 1998 Convergence Orders Estimates of Meshless Collocation Methods Using Radial Basis Functions *Adv. Comput. Math.* **8** 381-99
[36] Zhang X, Song K Z, Lu M W, and Liu X 2000 Meshless Methods Based on Collocation with Radial Basis Functions *Comput. Mech.* **26** 333-43
[37] Wang J G and Liu G R 2002 On the Optimal Shape Parameters of Radial Basis Functions Used for -2D Meshless Methods *Comput. Methods Appl. Mech. Eng.* **191** 2611-30
[38] Lee C K, Liu X and Fan S C 2003 Local Multiquadric Approximation for Solving Boundary Value Problems *Comput. Mech.* **30** 396-409
[39] Biazar J and Hosami M 2016 Selection of an Interval for Variable Shape Parameter in Approximation by Radial Basis Functions *Advances in Numerical Analysis* **2016** 1-11
[40] Franke R 1982 Scattered Data Interpolation: Tests of Some Method *Math. Comput.* **38** 181-200